Preparation and release behavior of poly(methyl methacrylate-co-methacrylic acid)-based electrospun nanofibrous mats loaded with doxorubicin

Roberto López-Muñoz, Raúl Guillermo López, Hened Saade, Angel Licea-Claverie, Francisco Javier Enríquez-Medrano, Graciela Morales, Daniel Grande

Preparation and release behavior of poly(methyl methacrylate-*co*-methacrylic acid)-based electrospun nanofibrous mats loaded with doxorubicin

Roberto López-Muñoz[a], Raúl Guillermo López[a], Hened Saade[a], Angel Licea-Claverie[b], Francisco Javier Enríquez-Medrano[a], Graciela Morales*[a], Daniel Grande[c]

[a]*Centro de Investigación en Química Aplicada, Blvd. Enrique Reyna, 140, 25294 Saltillo, Mexico.*

[b]*Centro de Graduados e Investigación en Química, Tecnológico Nacional de México/Instituto Tecnológico de Tijuana, 22414 Tijuana, Mexico.*

[c] *Univ Paris Est Creteil, CNRS, Institut de Chimie et des Matériaux Paris-Est (ICMPE), UMR 7182, 2, rue Henri Dunant, 94320 Thiais, France.*

Submitted as a regular article to *Polymer Bulletin*

*Correspondence author:

Graciela Morales

Phone: +52 844 4389830 Ext. 1230

E-mail: graciela.morales@ciqa.edu.mx

ABSTRACT

A drug-loaded electrospun mat is a potential fibrous material for cancer treatment after a surgery procedure. In this study, the poly(methyl methacrylate-*co*-methacrylic acid) [P(MMA-*co*-MAA)] copolymer was synthesized by semi-continuous heterophase polymerization as a nanofiber carrier to load an anticancer drug, doxorubicin hydrochloride (DOX). Eudragit® S100 (ES100) nanofibers loaded with DOX were also prepared for comparison. The electrospun nanofibers were loaded at different DOX concentrations, where the homogeneous fiber morphology did not change with the drug loaded increase. The confocal microscopic images indicated that the drug was incorporated to a major extent into the synthesized copolymer than the ES100 nanofibers, through electrostatic interactions or hydrogen bonding. The *In-vitro* release profiles of DOX presented a lower release rate for the synthesized copolymer around 12 % after 72 h, compared to 44 % released from ES100 copolymer. Both copolymers presented a two-stage diffusion-controlled mechanism, which obeyed Fick's second law. Based on these results, the synthesized methacrylic copolymer exhibited a high potential to release the drug in a sustained and prolonged manner. Thus, P(MMA-*co*-MAA) DOX-loaded electrospun mats have the potential to be used as local implantable fibrous material for postsurgical cancer treatment.

Keywords: methacrylic copolymers, electrospun nanofibers, doxorubicin, drug delivery, Eudragit® S100

1. INTRODUCTION

The primary goal of a drug delivery system (DDS) is to be able to direct a therapeutic agent in the body to the affected area and to control the rate of release in a sustained manner. For this, it is necessary to find an optimal formulation or a suitable device that allows such targeted action. However, the antineoplastic treatments commonly used like radiation, surgery, immunotherapy, thermotherapy, phytotherapy, gene therapy, and chemotherapy, affect healthy cells at different levels, thus causing well-known side effects [1]. For solid tumor diseases, the most common strategy is surgical removal, followed by one of the aforementioned treatments. In this context, most of the research works have been focused on strategies able to attack cancer cells in different ways, either to completely destroy them or to avoid their growth. In this regard, ultrafine polymeric nanofibers (NFs) containing antineoplastic agents have emerged as a promising option for preventing local tumoral cell recurrence after a tumor extraction by surgery [2]. Furthermore, moderate and sustained release over time of the antineoplastic agent is sought, in order to avoid side effects related to a burst release and high drug concentration.

Electrostatic spinning or electrospinning is an electro-hydrodynamic process by which polymeric fibers with diameters in the sub-micrometer down to nanometer range can be produced using a wide variety of natural or synthetic polymers solutions. The obtained fibers exhibit several interesting and advantageous characteristics, including large surface area to mass or volume ratio that promotes the efficient delivery of hydrophilic/hydrophobic drugs, highly interconnected pores between depositing fibers of the electrospun mats, versatility for surface functionalization. When they are used as drug delivery carriers, they also present high drug loading and encapsulation efficiency, as well as the ability to modulate the drug release which in turn depends on a variety of parameters like fiber diameter, morphology, and porosity.

In recent years, several reports have appeared in the specialized literature regarding the use of NFs from biodegradable polymers that are accepted for their use in humans, as carriers of antineoplastic drugs. Among them, doxorubicin is one of the first-line antineoplastic drugs used for a wide range of cancers like breast, prostate, ovarian, testicles, lung, bladder, stomach, and other cases like solid tumors, leukemia, and Kaposi sarcoma [3]. One of the first reports was that of Zeng *et al.* [4], who documented the preparation of NFs of poly(L-lactic acid) (PLLA) containing doxorubicin hydrochloride (DOX) and paclitaxel to give loaded NFs with mean diameters between 0.4 and 1 μm. The release tests indicated that DOX-loaded NFs exhibited

the highest release rate. Xu *et al.* prepared NFs based on poly(ethylene glycol)-poly(L-lactic acid) of about 0.5 μm in mean diameter, containing DOX [5], and a blend of DOX and paclitaxel [6]. The authors found that at higher drug concentrations, the release rate was slow, and that of paclitaxel was even slower than that associated with DOX, due to the compatibility between the polymer and the drug. Later, PLLA-based NFs were used for loading DOX [7,8], and specifically, Qiu *et al.* [8] prepared first silica nanoparticles loaded with DOX to later incorporate them into the precursory fiber solution, and a very slow release rate of DOX was found during the release studies.

NFs of poly(lactic-*co*-glycolic acid) containing DOX loaded into hydroxyapatite nanorods [9] and DOX loaded into layered nanohydroxyapatite [10] were prepared. The results obtained in the corresponding release tests showed that the drug was released in a very slow rate. Other interesting report is that of Dai *et al.* [11], who prepared poly(lactic acid) NFs containing a blend of DOX and natural pearl powder in order to obtain a material that simultaneously would release an antineoplastic drug and act as a scaffold for tissue growth. More recently, Gohary *et al.* [12] prepared NFs of poly(ε-caprolactone)/poly(ethylene oxide) blend containing silica nanoparticles previously loaded with DOX. The results showed a very slow release of the drug of only 35 % in 780 h. On the other hand, Radmansouri *et al.* [13], reported chitosan NFs loaded with cobalt ferrite nanoparticles and DOX for combining chemotherapy and hyperthermia. It is noteworthy that a common characteristic in all the reports mentioned above lies in the use of the electrospinning technique to obtain drug-loaded NFs.

Regarding the use of different polymer-based nanofibers to release anticancer drugs, the use of targeted release formulations is a common way to ensure that the drug can be freed only in a localized zone of the body where cancer cells are present. In this sense, one such family of materials correspond to the pH-sensitive polymers, and among them, the pH-responsive Eudragit® methacrylic copolymers. Drug release profiles provided by Eudragit®-based DDS include time-controlled release, colon-targeted release, and sustained release [14–16]. Eudragit® L100, L100-55, and S100 are specifically designed for targeting the lower parts of the gastro-intestinal tract; these polymers are insoluble at low pH, dissolving only at pH 6.0, 5.5, or 7.0, respectively. Eudragit® L100-55 was used by Shen *et al.* [15] to prepare electrospun fibers containing sodium diclofenac with an increase in the drug release from less than 3 % to total release when pH varied from 1.0 to 6.8, respectively. Similar results were observed by Yu *et al.* for the same copolymer with ketoprofen [17], helicid [18], or by Illangakoon *et al*. with

mebeverine hydrochloride [19]. Eudragit® S100 fibers containing uranine and nifedipine have shown to give rapid release of the incorporated drugs at pH 6.8, however no *In-vitro* studies were performed at lower pH values [20].

Furthermore, there are very few studies related to methacrylic fibrous materials for DDS, and they are even scarcer for cancer treatment. For instance, these studies used different polymers from the Eudragit® family, which have been loaded with 5-Fluorouracil [21], paclitaxel [22], or moxifloxacin hydrochloride [23]. To the best of our knowledge, and despite its recognition as a biocompatible material approved by the FDA for human intake, there are no reports concerning Eudragit® S100 [poly(methyl methacrylate-*co*-methacrylic acid) in a 2:1 MMA:MAA molar ratio] as the fibrous material, containing DOX as the anticancer drug.

Based on the background previously described, the main objective of the present study is to describe the preparation of DOX-loaded Eudragit® S100 nanofibers as polymer models, and those based on a methacrylic copolymer of different molar mass but with the same chemical composition, synthesized in our laboratories, by the electrospinning technique, meant for colon targeted delivery. The influence of molar mass on nanofibers formation, drug loading, and *In-vitro* drug release is investigated.

2. EXPERIMENTAL SECTION

2.1. Materials

For the copolymer synthesis, sodium dodecyl sulfate (SDS, 98.5 %), sodium bis(2-ethylhexyl) sulfosuccinate (AOT, 96 %), and ammonium persulfate (APS, 99 %) were purchased from Sigma-Aldrich (Toluca, México) and were used as received. Methyl methacrylate (MMA) and methacrylic acid (MAA) also from Sigma-Aldrich, were purified using a prepacked column for removing monomethyl ether hydroquinone (MEHQ). Doxorubicin hydrochloride (DOX) was purchased from MedChemExpress USA, New Jersey, and was used as received. Eudragit® S100 (ES100) was supplied by Evonik Nutrition & Care GmbH, Germany. Ethanol and dimethylformamide (DMF) were purchased from Sigma-Aldrich and used as received.

2.2. Synthesis of P(MMA-*co*-MAA) copolymer

A full detailed synthesis procedure was published in a previous report [24]. In brief, the polymerization was conducted using a 600 mL jacketed glass reactor equipped with a reflux condenser and mechanical steering using the following reactants: 465.5 g of water, 0.5 g of

APS, 3.5 g of SDS, and 1.5 g of AOT. All the reactants were charged into the reactor and the mixture was subjected to 530 rpm at 70 °C. The reaction was initiated with the addition of the monomer mixture in two steps to complete a final dosage of 62 g of MMA/MAA (2:1 molar ratio). The addition was carried out at a constant flow of 55.5 mL/h for 1 h using a dosing pump (Kd Scientific-100). The reactivity ratio of methyl methacrylate (r_2) is comprised between 0.2 to 0.4, while that corresponding to methacrylic acid (r_1) is around twice as high [25]. At the end of the dosing period, the polymerization was allowed to continue for 30 min and the reaction was finalized by cooling the reactor, yielding the product as a stable white latex. The evolution of instantaneous and global conversions with time and the corresponding characterization of this copolymer are reported in previous publications [24, 26-28].

2.3. Electrospinning precursory solutions, DOX loading, and spinning conditions

The latex obtained was treated in a Mini Spray Dryer *B-290* (Buchi equipment) with an inlet temperature of 190 °C and outlet temperature of 73 °C, working at 90 % aspirator and 40 % pumping, to obtain the corresponding copolymer powder.

In order to obtain homogeneous and smooth nanofibers during the electrospinning process, solutions at 12 and 6 wt.-% of ES100 and P(MMA-*co*-MAA), respectively, in an ethanol/DMF mixture (70/30 vol. and 65/35 vol.-%, respectively) were prepared. The different polymer concentrations and solvent mixture ratios were due to the difference in molar mass between both polymers ($\overline{Mn}_{\mathrm{ES100}}$ = 50,000 g mol^{-1}, $\overline{Mn}_{\mathrm{P(MMA-}co\mathrm{-MAA)}}$ = 200,000 g mol^{-1}. This difference in molar mass was corroborated by size-exclusion chromatography (SEC, see Supplementary Information, Figure S1), where the copolymer was previously treated with a methylating agent (trimethylsilyl diazomethane) to promote substitution of the polar group from methacrylic acid with a methyl group, thus allowing the copolymer to be solubilized in THF to perform the analysis. The spinning solutions of ES100 and the synthesized copolymer were prepared by first dissolving the corresponding polymer amount in 15 mL of ethanol/DMF.

To obtain DOX-loaded mats, the polymer amount for each formulation was first mixed in solid-state with different DOX concentrations of 3, 5, and 10 wt.-% (as compared with polymer content), and then 15 mL of the corresponding ethanol/DMF mixture was added. All the samples were stirred under dark conditions for 12 h. The fibrous materials were obtained with a FLUIDNATEK by Bioinicia equipment and the electrospinning process was subjected to the

following conditions: flow rate of 1 mL h^{-1}, a voltage of 20 kV, plate collector, and needle-to-plate collector distance of 15 cm.

Drug loading content (DLC) was determined by taking into account the mass ratio of DOX in the electrospun mat (M_{DOXf}) and the mass of the electrospun mat (M_{NFs}) for each formulation, according to Equation (1). Drug loading efficiency (DLE) was determined by the ratio of M_{DOXf} and the mass of DOX initially added in the polymer solution (M_{DOXo}), according to Equation (2). The samples were completely dissolved in 1 mL of methanol and vigorously mixed by using ultrasound with 3 mL of phosphate buffer solution (PBS) at pH 7.4. The mixtures were analyzed in an Ultraviolet/Visible (UV/Vis) spectrophotometer SHIMADZU UV-2401PC. The DOX concentration in the electrospun mats was calculated by triplicate measurements of absorbance at 483 nm using a drug calibration curve in PBS at pH 7.4.

$$DLC(\%) = \frac{M_{DOXf}\ \ (mg)}{M_{DOXf} + M_{NF}\quad (mg)} \times 100\ \% \tag{1}$$

$$DLE(\%) = \frac{M_{DOXf}\ \ (mg)}{M_{DOXo}\ \ (mg)} \times 100\ \% \tag{2}$$

2.4. Characterization techniques

2.4.1. Viscosity Measurements

The linear viscoelastic properties of the precursory solutions were measured in the Anton Paar rheometer, Physica MCR 301 model, using a set-up of concentric cylinders double-gap at room temperature.

2.4.2. Morphological analyses

The morphological analysis of the nanofibers was carried out using a field-emission scanning electron microscope (FE-SEM) with an electrical high tension (EHT) of 3.0 kV, and all the samples were previously coated with gold/palladium in a Cressington sputter coating equipment. The images were analyzed with the *Image J* software to estimate average fiber diameters ($\overline{D}_f$). Diameter distributions were obtained by measuring 400 fibers (using 5 different SEM images). Obtained data were represented by means of box-bars charts, where the boxes reflected 50 % of the population of values located between quartile 1 (Q_1 = 25 % of the

population) and 3 (Q_3 = 75 % of the population), while the bars represented the amplitude of the distribution according to the most probable values or those that appeared more frequently.

2.4.3. Contact angle measurements

To assess the hydrophobicity of the mats, the contact angles of the electrospun mats were measured using a Kruss EasyDrop goniometer at ambient temperature with distilled water (d-water). For these measurements, 5 d-water drops of 10 µL each were put on a rectangle of electrospun mat and the angle formed between the surface of the mat and the water drop was measured using a monochrome interline CCD (25/30 fps) camera.

2.4.4. Thermal analyses

Thermal properties were evaluated through thermogravimetric analysis (TGA) (TA Instruments, Q400) and differential scanning calorimetry (DSC) (TA Instruments, Q200). To perform TGA, the samples were heated from 30 to 600 °C under a nitrogen atmosphere, at a heating rate of 10 °C min^{-1} and then under oxygen flow up to 800 °C. Regarding DSC, the heating was carried out from room temperature to 200 °C at a heating rate of 10 °C min^{-1}, the samples were isothermally maintained at 200 °C for 2 min, and then cooled down at the same rate to −70 °C. A second heating cycle under the same conditions was conducted.

2.4.5. FTIR spectroscopy

Attenuated total reflectance Fourier transform infrared (FTIR) analysis was carried out on a Nicolet iS50 spectrophotometer (ThermoFisher Scientific) in transmittance mode. The scanning range was equal to 1800 - 650 cm^{-1}. 25 scans were registered, and the resolution was set at 1 cm^{-1}.

2.4.6. Fluorescent confocal tests

The distribution and dispersion of DOX were determined through the fluorescence emission of nanofibers loaded with DOX using a Zeiss LSM700 confocal laser scanning microscope that comprised an upright Zeiss Axio Imager Z1. The nanofibers loaded with different concentrations of DOX were excited at 550 nm, and the emission spectra were recorded at the same wavelength.

2.4.7. UV-Vis spectroscopy

UV-Vis spectra were obtained using a Shimadzu UV-2401PC spectrophotometer at room temperature with a dual-beam light source lamp of xenon and deuterium. The measurements were taken at medium scanning speed and spectral bandwidth of 1 nm.

2.4.8. In-vitro release studies

For the release studies, all the electrospun mats were cut in disk shapes of 12 mm diameter with 10 mg average mass (by triplicate). The DOX loaded NFs materials were dispersed in 3 mL of PBS at pH 7.4 using an ultrasonic bath and then put into a dialysis tube (Spectra/Pro® MWCO: 3.5 kDa, diameter 10 mm, from Spectrum™). The dialysis tubes were introduced into 50 mL of PBS solution inside amber flasks. The flasks were put inside a temperature-controlled bath at 37 °C under 500 rpm magnetic stirring. 3 mL aliquots of the medium were taken at different predetermined periods of time and replaced by 3 mL of fresh PBS solution at every sampling point. The released fraction of DOX was quantified from UV measurements at λ_{max} 483 nm using a calibration curve of DOX in PBS.

3. RESULTS AND DISCUSSION

3.1. Rheological study of ES100 and P(MMA-*co*-MAA) solutions at different copolymer concentrations and solvent ratios

Rheological studies of the polymer solutions corresponding to ES100 and P(MMA-*co*-MAA) copolymers were carried out in order to evaluate the apparent viscosity as a function of the shear rate at different polymer concentrations and solvent ratios (ethanol/DMF). For the ES100 system, the polymer concentration was varied from 4 to 14 wt.-%, while for the P(MMA-*co*-MAA) system, the concentration ranged from 4 to 10 wt.-%. These concentrations were taken based on solubility tests and the difference in molar masses of copolymers. Although polymers generally exhibit a pseudo-plastic behavior, characterized by a decrease in viscosity as the shear rate increases, in the case of the ES100 systems, characteristics of a Newtonian fluid were observed in all the samples, while for P(MMA-*co*-MAA) systems, the solutions showed a slight tendency towards a pseudo-plastic behavior beyond 7 wt.-% concentrations.

Likewise, the concentration regimes in which the polymer solutions of both systems promoted the formation of homogeneous fibers were determined, by measuring the zero-shear viscosity (η_o) in the region of linear viscoelasticity for all solutions (Figures 1a, b). The η_o values were

plotted as a function of polymer concentration (Figure 1c) in order to evidence a significant slope change, associated with the entanglement degree of polymeric chains. These results showed, on the one hand, that the different solvent ratio for the ES100 and P(MMA-*co*-MAA) solutions did not show a significant change in the viscosity curves. However, the ES100 systems prepared with an 80/20 solvent ratio (ethanol/DMF) did not show signs of precipitation with respect to time, unlike the solutions prepared with a 70/30 ratio, which precipitated after 4 h. On the other hand, the P(MMA-*co*-MAA) system showed similar behavior, precipitating the copolymer after 2 hours with a 50/50 solvent ratio, unlike the 65/35 ratio solutions, which did not present precipitation. Taking into account these results the following conditions were selected for the electrospinning process: 12 wt.-% of ES100 in ethanol/DMF 70/30 vol.-%, and 6 wt.-% of P(MMA-*co*-MAA) in ethanol/DMF 65/35 vol.-%. The same conditions were used during the electrospinning process of polymer solutions in the presence of DOX for both systems.

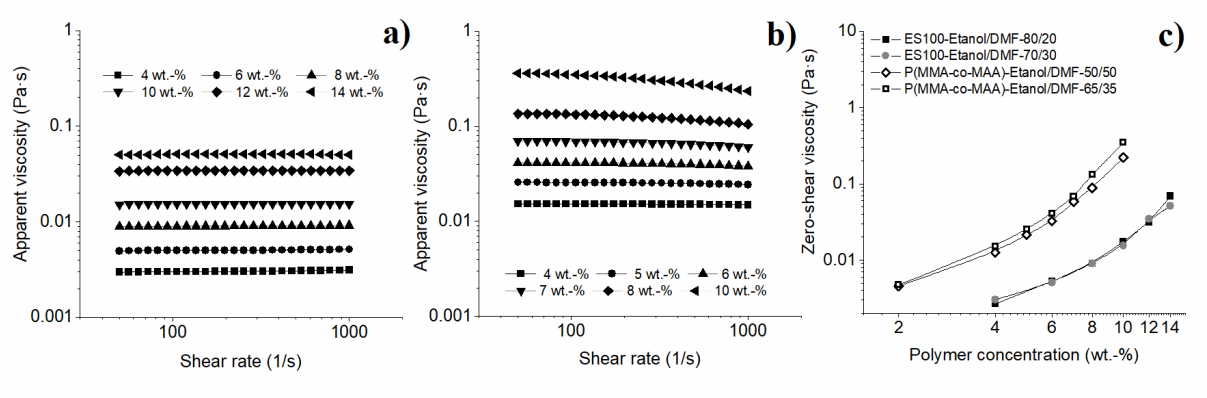

Fig. 1 Rheological studies of (a) ES100 and (b) P(MMA-*co*-MAA) solutions at different polymer concentration, (c) Dependence of zero-shear viscosity (η_o) on polymer concentration.

3.2. Effect of DOX on fiber formation

The morphology and the average diameters ($\overline{D}_f$) of fibers without and with loaded DOX are discussed in this section. In the latter case, the electrospinning solutions of P(MMA-*co*-MAA)/DOX did no present heterogeneity or phase separation, indicating that the drug was homogeneously dispersed. However, those prepared with ES100 presented a small DOX precipitation after 5 h during the electrospinning process. Despite this, all the electrospun fibers (with and without DOX) are mostly smooth, continuous, and homogeneous (*i.e.* no beads were observed) throughout the length of the fibers (Figures 2a-d, and see Supplementary Information, Figures S2, S3).

The $\overline{D_f}$ values of ES100/DOX NFs were equal to 350 and 370 nm, while for P(MMA-*co*-MAA)/DOX fibers, the $\overline{D_f}$ values were equal to 450 and 570 nm. Such values were similar to those reported for 50 % of the population of the fibers without the drug (Figures 2e, f), where $\overline{D_f}$ for the unloaded fibers were 300 and 450 nm for ES100 and P(MMA-*co*-MAA), respectively. These results corroborated the differences observed in rheological studies, in which an increase in apparent viscosity of almost two orders of magnitude was observed for P(MMA-*co*-MAA) with a concentration of 6 wt.-% ($\overline{D_f}$ = 570 nm), associated with the highest molar mass, compared to ES100 with a concentration of 12 wt.-% ($\overline{D_f}$ = 370 nm). Thus, it could be inferred that the presence of the drug did not promote significant changes in the viscosity of the precursory solutions. On the other hand, the difference in $\overline{M_n}$ values could promote a higher load efficiency due to the presence of a higher content of carboxylic groups in the polymer chains that could be linked to the drug by electrostatic interactions or hydrogen bonding.

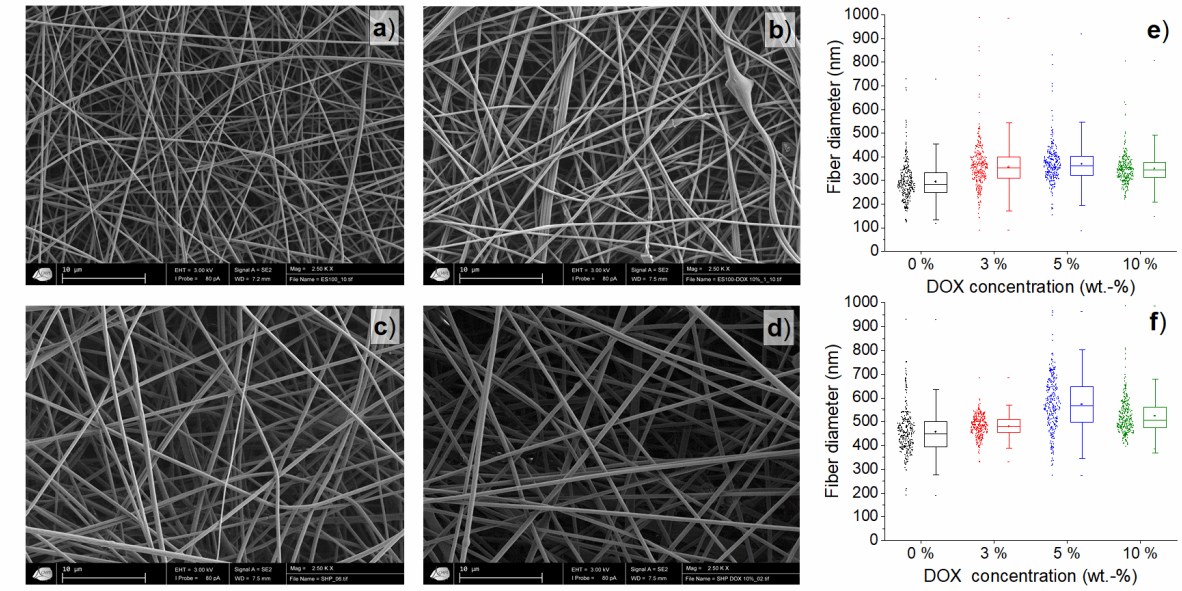

Fig. 2 SEM images; (a) ES100 nanofibers, (b) ES100 with 10 wt.-% DOX, (c) P(MMA-*co*-MAA) nanofibers, (d) P(MMA-*co*-MAA) with 10 wt.-% DOX, (e) Fiber diameters of ES100 at different DOX concentrations, (f) Fiber diameters of P(MMA-*co*-MAA) NFs at different DOX concentrations.

3.3. Characterization of fibers loaded with DOX

The quantification of the DOX content in the fibers of ES100 and P(MMA-*co*-MAA) was carried out by means of the calibration curve of the drug in the phosphate solution (PBS) at pH 7.4, where the samples were completely dissolved, via UV-Vis measurements (see

Supplementary Information, Figure S4). The values of drug loading content (DLC) and drug loading efficiency (DLE) are summarized in Table 1 where the standard deviation (SD) is also indicated in each case.

Table 1 Drug loading content (DLC) and drug loading efficiency (DLE) of DOX in methacrylic nanofibers.

Copolymer	Theoretical DOX (wt.-%)	DLC (wt.-%)	SD (%)	DLE (wt.-%)	SD (%)	[DOX] (mg/mm^2)	SD (mg/mm^2)
ES100	3	1.84	0.077	61.28	2.58	1.78	4.8E-3
	5	3.91	0.407	78.19	8.15	3.88	2.7E-2
	10	6.54	0.339	65.39	3.39	6.43	2.0E-2
P(MMA-*co*-MAA)	3	2.80	0.165	93.42	5.51	2.66	0.157
	5	4.34	0.301	86.76	6.02	4.12	0.286
	10	7.16	0.446	71.61	4.46	6.81	0.424

These results suggested that there was a better incorporation of the drug in the P(MMA-*co*-MAA) copolymer, possibly due to the presence of a higher content of carboxylic groups (associated with the higher molar mass) that promoted electrostatic interactions and hydrogen bonds, in comparison with ES100 fibers. In the case of ES100-based NFs with 5 wt.-% DOX, the system would be close to the optimal loading value to maximize efficiency, meanwhile for P(MMA-*co*-MAA) NFs the highest DLE was obtained with 3 wt.-% DOX loading.

3.4. Contact angle measurements on electrospun methacrylic fibers

In the biomedical and pharmaceutical fields, the wettability is an important parameter since it can describe the interaction that a solid system (electrospun mats) may have with different physiological fluids. Thus, contact angle (θc) measurements of the different mats obtained were performed in order to analyze the effect that DOX might have on nanofibers surface. Values of θc lower than 90° indicate hydrophilic interactions between the solid surface and the dissolution medium, values of θc between 90° and 150° correspond to hydrophobic interactions, meanwhile θc higher than 150° is indicative of super-hydrophobic interactions [29,30].

From the values reported in Figure 3, ES100-based fibers showed a hydrophobic behavior. θc values increased with DOX concentration from 118° for pristine ES100 to 124° for the same mat loaded with 10 wt.-% of DOX, where in addition the d-water drop kept its shape for more

than 2 min. This behavior could probably be attributed to a poor interaction/distribution of DOX molecules in the polymer matrix, according to literature [9,31].

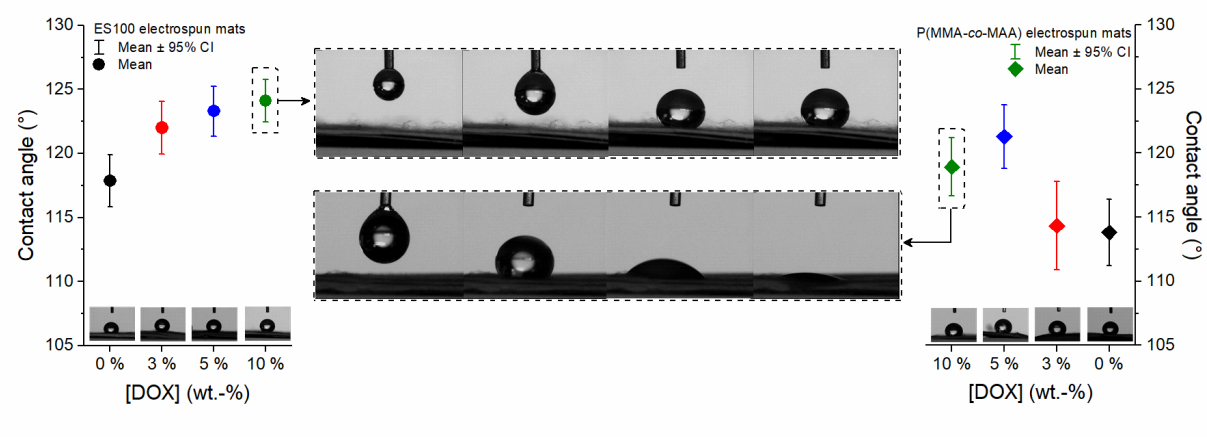

Fig. 3 Contact angle values of electrospun nanofibers based on ES100 and P(MMA-*co*-MAA) loaded with different DOX concentrations. The photographs correspond to the water drop falls on the corresponding mats loaded with 10 wt.-% of DOX.

Regarding the mats prepared with P(MMA-*co*-MAA), that obtained without DOX showed a θc equal to 114°, while the mats with 10 wt.-%. DOX presented a θc value equal to 118° (see Figure 3). However, the d-water drop on the P(MMA-*co*-MAA) mat kept its shape just for a few seconds, *i.e.* a time period enough to take a snapshot and measure the contact angle. Even though the contact angle values also indicated a hydrophobic behavior for P(MMA-*co*-MAA)/DOX, these values were lower than those for ES100. The contact angle values showed an irregular behavior due to the rapid collapse of the drop during the analysis. On the other hand, as P(MMA-*co*-MAA) was not subjected to a dialysis process after the synthesis in order to remove the surfactants, the presence of SDS and AOT within the fibers, could affect the surface tension of the water drop in the measurements of the contact angles causing its rapid collapse. The electrical conductivity measurements of the precursory solutions used to obtain the fibers could corroborate the presence of surfactants on the electrospun systems (Table 2). The difference in electrical conductivity values between ES100 and P (MMA-*co*-MAA) of 62 to 239 µS/cm respectively, could be attributed to the anionic molecules of both surfactants (*i.e.*, SDS and AOT).

Table 2 Electrical conductivity measurements of precursory solutions at different polymer contents.

Polymer in Ethanol/DMF	Polymer content (wt.-%)	Electrical conductivity (µS/cm)
ES100	10	59.20
	12	62.18
	14	ND
P(MMA-*co*-MAA)	4	254.40
	6	328.60
	8	ND

ND: Not determined due to high viscosity.

3.5. Thermal analysis of electrospun methacrylic fibers

From the thermo-degradation patterns of the scaffolds formulated with ES100 and P(MMA-*co*-MAA) without and with 10 wt.-% DOX (Figure 4), it could be observed around 20 % mass loss from 100 °C to 400 °C, attributed to water and methanol loss through intermolecular reactions between monomer units, promoting anhydrides formation. Chain scission and depolymerization of MMA unit sequences generally occur above 300 °C [32]. The mass loss from 400 to 450 °C could be related to the decomposition of the polymer matrix.

Although the degradation temperature of these materials is much higher than the temperatures to which they would be exposed, the effect of the presence of DOX could be observed, where considering the degradation rate at its maximum value (T_d) obtained by the derivative of the thermogram (Table 3), DOX produced an increase in the thermal stability of ES100-based mats, contrary to the mats based on P(MMA-*co*-MAA) where no significate variations were observed.

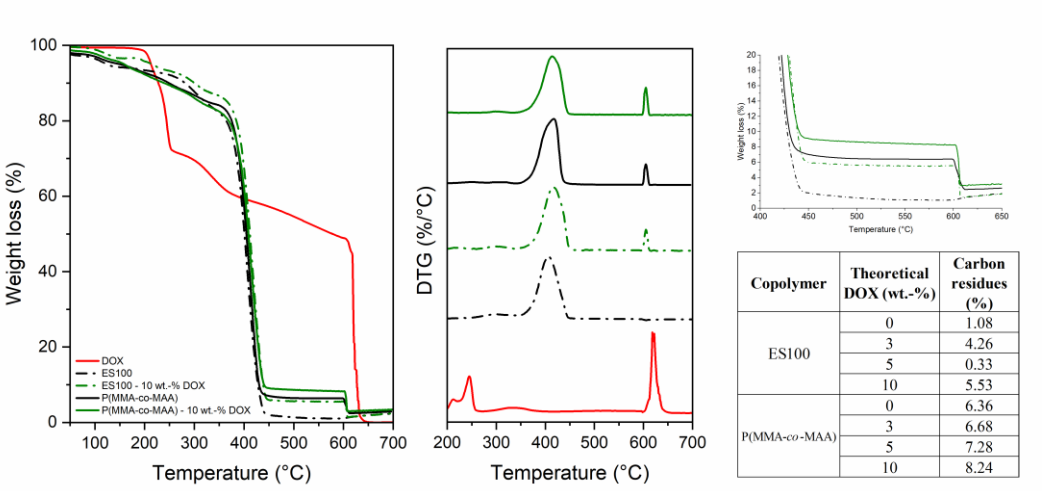

Copolymer	Theoretical DOX (wt.-%)	Carbon residues (%)
ES100	0	1.08
	3	4.26
	5	0.33
	10	5.53
P(MMA-*co*-MAA)	0	6.36
	3	6.68
	5	7.28
	10	8.24

Fig. 4 Degradation patterns derived from TGA analysis of the electrospun fibers based on pristine ES100 and P(MMA-*co*-MAA) as well as the corresponding 10 wt.-% DOX loaded fibers.

Table 3 Thermal decomposition temperature (T_d) and glass transition temperature (T_g) of different obtained mats.

Fibrous material	Theoretical DOX content (wt.-%)	T_d (°C)	T_g (°C)
ES100	0	407	143
	3	410	145
	5	413	147
	10	416	145
P(MMA-*co*-MAA)	0	417	134
	3	414	137
	5	408	136
	10	414	137

On the other hand, the increase in carbon residues at 600 °C before changing from nitrogen flow to oxygen from 4.2 to 5.5 % for ES100 and from 6.7 to 8.2 % for P(MMA-*co*-MAA), could be due to drug residues loaded into the electrospun nanofibers. In both cases, these values did not match with the theoretical values of DOX loading, where the non-homogeneous distribution of DOX within the fibers should be considered.

Regarding DSC results (Figure 5), the addition of DOX into the polymeric fibers influenced the macromolecular chains allowing them to be more rigid, thus leading to slightly higher T_g values. On the other hand, DOX has a melting point (T_m) at 205-206 °C resulting in an endothermic

peak in the DSC curve, thus evidencing the presence of crystals in the drug. The absence of the characteristic melting peak of the drug in the DSC curves for both loaded mats suggested that the DOX present in the fibers became an amorphous phase and that all the added drug is bound to the polymer backbone as reported by other authors [33].

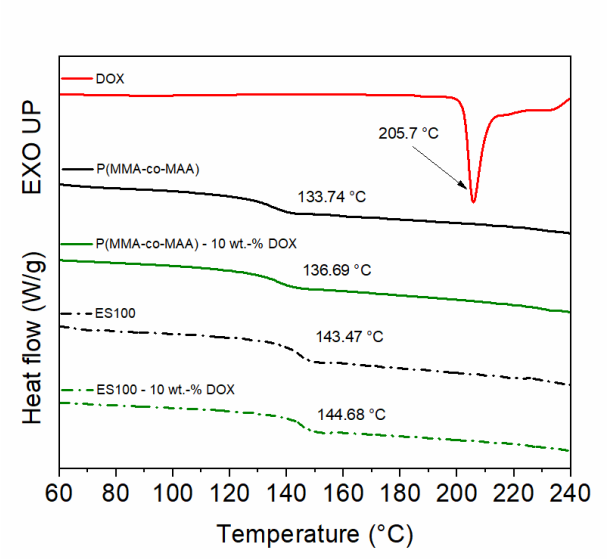

Fig. 5 DSC thermograms of ES100 and P(MMA-*co*-MAA) fibrous mats without and with 10 wt.-% DOX.

3.6. FTIR spectroscopy investigation of DOX-loaded fibers

The DOX loading into the electrospun mats was confirmed by FTIR spectroscopy in transmittance mode, and the spectra bands most representative are presented in Figure 6. The DOX presence was more forcefully evidenced at the highest DOX concentration in each system with new bands between 1700 and 600 cm^{-1}. The broad bands from 3500 to 3100 cm^{-1} were related to O-H stretching vibrations from the methacrylic acid units, absorbed water, and overlapping ν(H–O) signals from aromatic rings of DOX molecules (see Supplementary Information, Figure S5). The broad band between 3160 and 2300 cm^{-1} was attributed to $\nu(NH_3^+)$ which was overlapped by copolymer bands.

The bands at 2990 and 2945 cm^{-1} were associated with antisymmetric and symmetric stretching vibrations of $\nu(CH_2)$ from copolymer backbone. The absorption band at 1580 cm^{-1} could be associated with ν(C=C) from aromatic rings of DOX, while the band at 1524 cm^{-1} was related to bending vibrations of δ(N–H). The small band at 1412 cm^{-1} was associated with δ(CH)

bending vibrations from aromatic rings. The last two bands at 990 and 805 cm^{-1} may be related to ν(C-O-C) stretching and ω(N-H) wagging vibrations, respectively. Most of the bands found in this study were in good agreement with those reported by Lanz-Landazúri *et al.* [34], where DOX was incorporated into poly(β, L-malic acid) (PMLA). FTIR results may indicate that the DOX amine group was directly involved in the association with carboxylic groups of the copolymers.

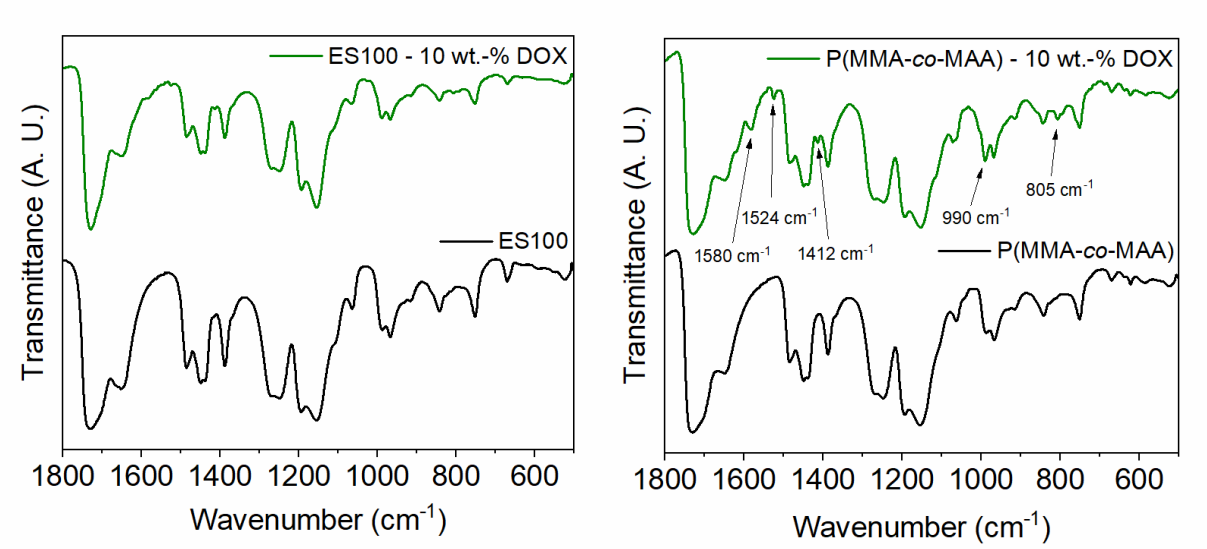

Fig. 6 FTIR spectra of pristine ES100 and P(MMA-*co*-MAA) electrospun mats as well as of the corresponding mats loaded with 10 wt.-% DOX.

3.7. Confocal fluorescent microscopy investigation of DOX-loaded fibers

The distribution of DOX within the electrospun fibers was observed through confocal fluorescence microscopy, and the results are shown in Figure 7. The ES100/DOX fibers exhibited slightly red fibers and small red-spot emissions that increased in size and color intensity with drug concentration (Figures 7a-c). The red spots could be attributed to DOX agglomerates that could not be attached to the polymer chains, due to a low concentration of carboxylic groups. Likewise, the slightly red-fluorescence emission may suggest a poor interaction between the hydrophobic drug and the polymer matrix, as previously demonstrated by contact angle measurements (see section 3.4). On the other hand, P(MMA-*co*-MAA)-based nanofibers exhibited a high-intensity red-fluorescence emission and fewer DOX agglomerates with drug concentration increment (Figures 7d-f). These results evidence an improvement in the distribution and incorporation of the cationic drug which could be attributed to a higher concentration of carboxylic groups in the polymer chains, thus favoring the affinity between

the drug and the polymeric matrix, along with a higher DOX loading, according to the loading efficiency results (see Table 1).

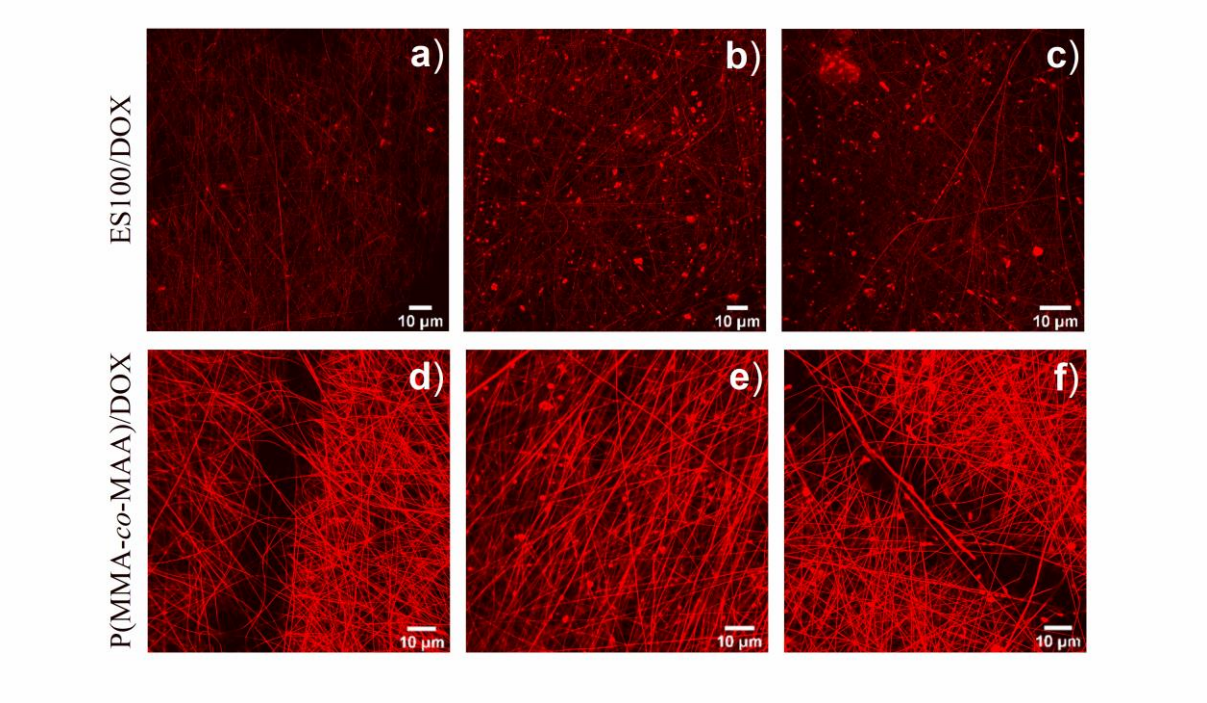

Fig. 7 Confocal fluorescence microscopy for ES100 and P(MMA-*co*-MAA) electrospun mats at 550 nm emission loaded with 3 wt.-% (a, d), 5 wt.-% (b, e), and 10 wt.-% (c, f) DOX.

The fluorescence results confirmed that DOX has a good distribution not only in the fiber core but also in their fiber surface. Similar results were reported by Xu *et al.* [5], where confocal microscopic images indicated that DOX was well incorporated into amphiphilic poly(ethylene glycol)-poly(L-lactic acid) diblock copolymer nanofibers. On the other hand, Park *et al.* [29] reported an immiscible behavior of DOX with poly(lactic acid) (PLA), where DOX was not soluble in the pre-spinning solution with dichloromethane and DMF, hence DOX particles were aggregated and precipitated in the solution. Due to the lack of compatibility between DOX and PLA, the electrospun fibers produced large aggregates (red-spot emissions), similar to those observed in the ES100 mats herein investigated.

3.8. *In-vitro* release of DOX from electrospun methacrylic fibers

The DOX release profiles from the ES100 NFs containing different concentrations of DOX are shown in Figure 8a. A burst release occurred in the first 9 h at pH 7.4, with about 12, 20, and 31 % DOX release, which corresponds to an average 7 mg DOX from the total drug content for

each formulation loaded with 3, 5, and 10 wt.-%, respectively (see Table 1). After this stage, there was a slowdown release rate in all cases of around 3 % every 24 h, reaching a release of about 17, 27, and 44 % at 72 h. Therefore, the release profiles showed a decrease in the release rate as the drug content in the NFs increased, which corroborated the trend reported in the literature [5,6,8,9].

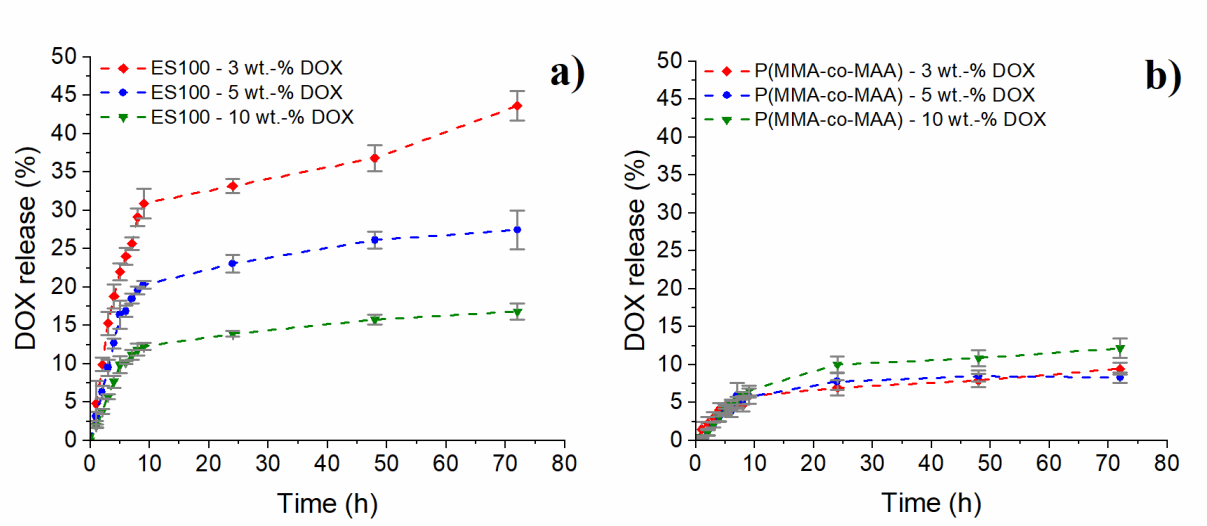

Fig. 8 *In-vitro* 3-day release profiles of DOX from methacrylic fibers. (a) ES100 electrospun mats, (b) P(MMA-*co*-MAA) electrospun mats.

The release profiles of the drug from P(MMA-*co*-MAA) NFs at different DOX concentrations are shown in Figure 8b. In this case, the release profiles showed a lower amount of released DOX in the first 9 h independently of the drug concentration, with about 7 % DOX release, which corresponds to an average of 3.4 mg DOX from the total drug content for each evaluated system (see Table 1). Similar to ES100-DOX release profiles, there was a slowdown release rate in all cases every 24 h of around 1 %, reaching a release close to 11 % at 72 h. However, the total drug released by the loaded P(MMA-*co*-MAA) NFs, especially those prepared with 3 and 5 wt.-%. DOX, was quite lower than that corresponding to their counterparts of ES100 NFs shown in Figure 8a. It is remarkable that unlike previous literature reports [5,6,8,9], the release profiles of the loaded P(MMA-*co*-MAA) NFs displayed an increase in the release rate as the drug content increased.

The release profiles for the electrospun mats loaded at 3 wt.-% for both methacrylic copolymers were extended for 20 days (see Supplementary Information, Figures S6, S7). The synthesized copolymer kept the release behavior during the 20 days, which could be attributed to the fact

that this electrospun mat did not solubilize in an aqueous solution at pH 7.4, retaining the drug for a longer period of time. On the other hand, the loaded ES100 mats presented a similar release behavior. However, after 72 h the DOX concentration decreased 7.4 % from the release medium. This fact suggests that a fraction of DOX could start degrading after 72 h as it was previously reported by Wu *et al*. [35], where an aqueous DOX solution was monitored at three different pH values for 50 h. The results showed that the DOX solution was less stable in basic conditions presenting an increase in the degradation rate at pH 7.4. Moreover, an increase in DOX concentration also promotes an increase in the degradation rate.

In order to elucidate the DOX release mechanism, Xu *et al.* [5] identified three stages during the release of DOX from poly(ethylene glycol)-poly(L-lactic acid) NFs, where the first two stages followed a Fickian type diffusion, that is, they fitted the Higuchi model [36]. By comparison, there seemed to be a similarity between the two stages observed in Figures 9a and 9b with the first two stages described in Xu's work [5]. As a matter of fact, the experimental data of each stage were fitted to a straight line according to the linearized equation of the Higuchi model represented by Equation (3) [36]:

$$Q = K_H\sqrt{t} \tag{3}$$

where Q is the cumulative percentage drug release at time t and k_H is the dissolution constant (see values in Table 4).

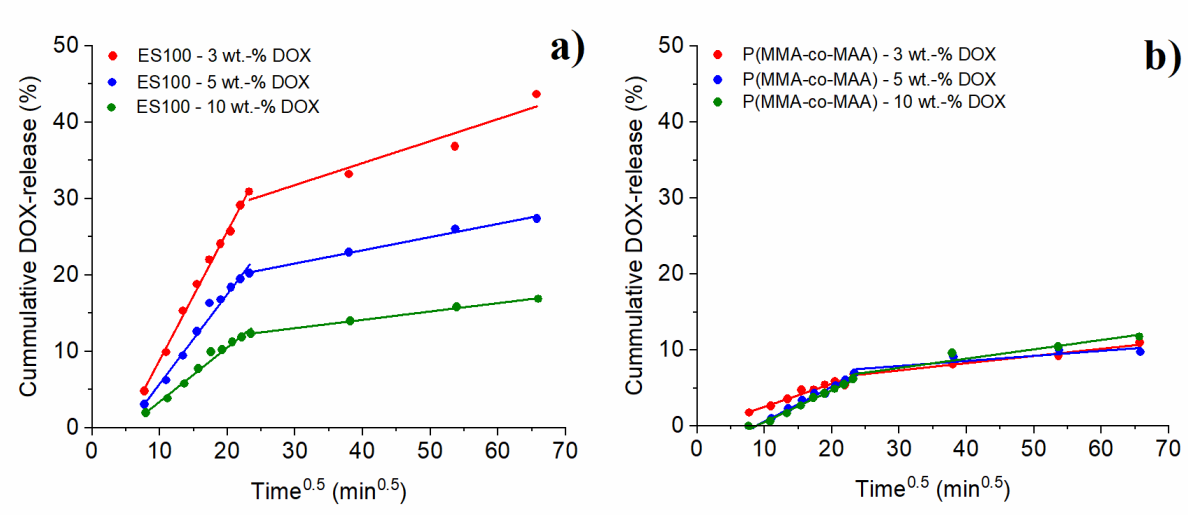

Fig. 9 Linear fitting of DOX released as a representation of Higuchi's model. (a) ES100/DOX fibers, (b) P(MMA-*co*-MAA)/DOX fibers.

Table 4 R-squared for each stage and diffusion constant (K_H) obtained from the fit with the Higuchi model of experimental data of DOX release from methacrylic electrospun fibers.

Copolymer	Theoretical DOX (wt.-%)	First stage (R^2)	Second stage (R^2)	First stage (K_H)
ES100	3	0.9948	0.8770	1.68
	5	0.9770	0.9847	1.17
	10	0.9768	0.9951	0.71
P(MMA-*co*-MAA)	3	0.9445	0.9662	0.30
	5	0.9890	0.6748	0.45
	10	0.9865	0.8696	0.42

The R^2 values for each stage from the fit of experimental data with the Higuchi model are shown in Table 4. In all cases, the experimental data fit with the Higuchi model for the first stage; however, in the second stage, the values presented a lower adjustment for 3 wt.-% DOX loaded in ES100 fibers (Figure 9a) and for higher load than 5 wt.-% DOX in P(MMA-*co*-MAA) fibers (Figure 9b). Taking into account this analysis, it might be concluded that at least during the two stages identified, the DOX would be released from NFs in accordance with the Higuchi model.

The drug released in the first stage for both systems could be related to the DOX located close to the NFs surface, while the drug release in the second stage could be related to the DOX contained within the NFs possibly by electrostatic interactions or hydrogen bonds. Nevertheless, it should be highlighted that in our study the DOX was released at lower rates than those reported in other works on polymeric NFs containing DOX [4–6], which should be beneficial for preventing cancer cell growth after the initial stage of burst drug release.

When comparing the results of the loading of ES100 and P(MMA-*co*-MAA) NFs and the corresponding release studies, some interesting points could be inferred. First of all, the loading efficiency, and consequently the drug load, was higher in P(MMA-*co*-MAA)-based NFs. Moreover, the fraction of DOX released at a predetermined period of time (72 h) was much lower in the case of P(MMA-*co*-MAA) NFs, mainly for the loaded NFs prepared with 3, and 5 wt.-% drug, and the release rate of DOX was significantly lower than those reported in other works on polymeric NFs containing DOX [4–6]. Since the MMA:MAA ratio was identical for both ES100 and P(MMA-*co*-MAA), the reason of the behavior described above could be

attributed to the larger size of the P(MMA-*co*-MAA) chains, where the entanglement of larger chains after they become insoluble during the spinning process favors the entrapment of drug molecules, thus hindering their release.

4. CONCLUSIONS

In summary, the electrospinning conditions for DOX-loaded methacrylic nanofibers based on ES100 and a copolymer with a similar composition synthesized by semi-continuous heterophase polymerization (SHP) were optimized to obtain homogeneous and smooth nanofibers. The DOX presence within the fibers was confirmed by several analyses, mainly by FTIR and confocal fluorescence microscopy studies. Drug incorporation did not affect the morphology and average fiber diameters with respect to those obtained without DOX. Moreover, the DLC was higher in case of P(MMA-*co*-MAA)-DOX systems, according to UV-Vis spectra and fluorescence results. These behaviors also suggested a better drug incorporation/interaction with the synthesized copolymer due to a higher content of carboxylic groups (associated with an increase in $\bar{M}_n$) that promoted a higher drug loading though electrostatic interactions or hydrogen bonds.

The *In-vitro* release comparison between DOX-loaded ES100 and P(MMA-*co*-MAA) nanofibers was investigated to develop a facile strategy for a sustained DOX release. The DOX molecules were better distributed in P(MMA-*co*-MAA) than ES100, possibly due to the difference in molar masses and carboxylic groups in the polymer chains. During the release process, the release rate of DOX decreased as the DOX content in the fibers increased, which could be attributed to the hydrophobic domain between PMMA fractions from the polymer chain and non-bonded DOX, whereas the DOX molecules located on the fiber surface were released first. The two sequential stages that represented the diffusion-controlled by Fick's second law for both systems evidenced a higher rate of DOX diffusion for ES100 fibers, possibly due to the poor drug distribution in the fibers, which leads to faster drug diffusion. Therefore, P(MMA-*co*-MAA)-DOX electrospun mats could have a better DOX release control with respect to Eudragit fibers, leading to materials with the suitable characteristics required for post-surgery cancer treatment.

ACKNOWLEDGEMENTS

The authors acknowledge *Consejo Nacional de Ciencia y Tecnología* (CONACyT) for PhD scholarship granted to R. López-Muñoz and for financial support through the project A1-S-

29092. Financial support from CNRS through French Mexican PICS program is gratefully acknowledged. The authors are also grateful to Myrna Salinas and María Guadalupe Méndez (CIQA, Mexico) for their technical assistance in the thermal characterization.

DECLARATION OF COMPETING INTEREST

The authors declare that they have no known competing financial interests or personal relationships that could have appeared to influence the work reported in this paper.

REFERENCES

[1] Shahbaz Aslam, M.; Naveed, S.; Ahmed, A.; Abbas, Z.; Gull, I.; Athar, M. A.; Aslam, M. S.: Side Effects of Chemotherapy in Cancer Patients and Evaluation of Patients Opinion about Starvation Based Differential Chemotherapy. Journal of Cancer Therapy, **5**, 817–822 (2014). http://doi:10.4236/jct.2014.58089.

[2] Bu, L. L.; Yan, J.; Wang, Z.; Ruan, H.; Chen, Q.; Gunadhi, V.; Bell, R. B.; Gu, Z.: Advances in drug delivery for post-surgical cancer treatment. Biomaterials, **219**, 119182 (2019). http://doi:10.1016/j.biomaterials.2019.04.027.

[3] Kwon, G.; Naito, M.; Yokoyama, M.; Okano, T.; Sakurai, Y.; Kataoka, K.: Block copolymer micelles for drug delivery: Loading and release of doxorubicin. Journal of Controlled Release, **48**, 195–201 (1997). http://doi:10.1016/S0168-3659(97)00039-4.

[4] Zeng, J.; Yang, L.; Liang, Q.; Zhang, X.; Guan, H.; Xu, X.; Chen, X.; Jing, X.: Influence of the drug compatibility with polymer solution on the release kinetics of electrospun fiber formulation. Journal of Controlled Release, **105**, 43–51 (2005). http://doi:10.1016/j.jconrel.2005.02.024.

[5] Xu, X.; Chen, X.; Ma, P.; Wang, X.; Jing, X.: The release behavior of doxorubicin hydrochloride from medicated fibers prepared by emulsion-electrospinning. European Journal of Pharmaceutics and Biopharmaceutics, **70**, 165–170 (2008). http://doi:10.1016/j.ejpb.2008.03.010.

[6] Xu, X.; Chen, X.; Wang, Z.; Jing, X.: Ultrafine PEG-PLA fibers loaded with both paclitaxel and doxorubicin hydrochloride and their in vitro cytotoxicity. European Journal of Pharmaceutics and Biopharmaceutics, **72**, 18–25 (2009). http://doi:10.1016/j.ejpb.2008.10.015.

[7] Liu, S.; Zhou, G.; Liu, D.; Xie, Z.; Huang, Y.; Wang, X.; Wu, W.; Jing, X.: Inhibition

of orthotopic secondary hepatic carcinoma in mice by doxorubicin-loaded electrospun polylactide nanofibers. Journal of Materials Chemistry B, **1**, 101–109 (2013). http://doi:10.1039/c2tb00121g.

[8] Qiu, K.; He, C.; Feng, W.; Wang, W.; Zhou, X.; Yin, Z.; Chen, L.; Wang, H.; Mo, X.: Doxorubicin-loaded electrospun poly(l-lactic acid)/mesoporous silica nanoparticles composite nanofibers for potential postsurgical cancer treatment. Journal of Materials Chemistry B, **1**, 4601–4611 (2013). http://doi:10.1039/c3tb20636j.

[9] Zheng, F.; Wang, S.; Shen, M.; Zhu, M.; Shi, X.: Antitumor efficacy of doxorubicin-loaded electrospun nano-hydroxyapatite- poly(lactic-co-glycolic acid) composite nanofibers. Polymer Chemistry, **4**, 933–941 (2013). http://doi:10.1039/c2py20779f.

[10] Luo, H.; Zhang, Y.; Yang, Z.; Zuo, G.; Zhang, Q.; Yao, F.; Wan, Y.: Encapsulating doxorubicin-intercalated lamellar nanohydroxyapatite into PLGA nanofibers for sustained drug release. Current Applied Physics, **19**, 1204–1210 (2019). http://doi:10.1016/j.cap.2019.08.003.

[11] Dai, J.; Jin, J.; Yang, S.; Li, G.: Doxorubicin-loaded PLA/pearl electrospun nanofibrous scaffold for drug delivery and tumor cell treatment. Materials Research Express, **4**, 075403 (2017). http://doi:10.1088/2053-1591/aa7479.

[12] Gohary, M. I. E.; Hady, B. M. A. El; Saeed, A. A. A.; Tolba, E.; Rashedi, A. M. I. E.; Saleh, S.: Electrospinning of doxorubicin loaded silica/poly(ϵ-caprolactone) hybrid fiber mats for sustained drug release. Advances in Natural Sciences: Nanoscience and Nanotechnology, **9**, aab999 (2018). http://doi:10.1088/2043-6254/aab999.

[13] Radmansouri, M.; Bahmani, E.; Sarikhani, E.; Rahmani, K.; Sharifianjazi, F.; Irani, M.: Doxorubicin hydrochloride - Loaded electrospun chitosan/cobalt ferrite/titanium oxide nanofibers for hyperthermic tumor cell treatment and controlled drug release. International Journal of Biological Macromolecules, **116**, 378–384 (2018). http://doi:10.1016/j.ijbiomac.2018.04.161.

[14] Shen, X. X.; Yu, D. G.; Zhu, L. M.; Branford-White, C.: Preparation and characterization of ultrafine Eudragit L100 fibers via electrospinning. 3rd International Conference on Bioinformatics and Biomedical Engineering, iCBBE 2009, , 9–12 (2009). http://doi:10.1109/ICBBE.2009.5163230.

[15] Shen, X.; Yu, D.; Zhu, L.; Branford-White, C.; White, K.; Chatterton, N. P.: Electrospun diclofenac sodium loaded Eudragit® L 100-55 nanofibers for colon-targeted drug delivery. International Journal of Pharmaceutics, **408**, 200–207 (2011). http://doi:10.1016/j.ijpharm.2011.01.058.

[16] Khan, M. Z. I.; Prebeg, Ž.; Kurjaković, N.: A pH-dependent colon targeted oral drug delivery system using methacrylic acid copolymers. I. Manipulation of drug release using Eudragit® L100-55 and Eudragit® S100 combinations. Journal of Controlled Release, **58**, 215–222 (1999). http://doi:10.1016/S0168-3659(98)00151-5.

[17] Yu, D. G.; Williams, G. R.; Wang, X.; Liu, X. K.; Li, H. L.; Bligh, S. A.: Dual drug release nanocomposites prepared using a combination of electrospraying and electrospinning. RSC Advances, **3**, 4652–4658 (2013). http://doi:10.1039/c3ra40334c.

[18] Yu, D. G.; Liu, F.; Cui, L.; Liu, Z. P.; Wang, X.; Bligh, S. W. A.: Coaxial electrospinning using a concentric Teflon spinneret to prepare biphasic-release nanofibers of helicid. RSC Advances, **3**, 17775–17783 (2013). http://doi:10.1039/c3ra43222j.

[19] Illangakoon, U. E.; Nazir, T.; Williams, G. R.; Chatterton, N. P.: Mebeverine-loaded electrospun nanofibers: Physicochemical characterization and dissolution studies. Journal of Pharmaceutical Sciences, **103**, 283–292 (2014). http://doi:10.1002/jps.23759.

[20] Hamori, M.; Yoshimatsu, S.; Hukuchi, Y.; Shimizu, Y.; Fukushima, K.; Sugioka, N.; Nishimura, A.; Shibata, N.: Preparation and pharmaceutical evaluation of nano-fiber matrix supported drug delivery system using the solvent-based electrospinning method. International Journal of Pharmaceutics, **464**, 243–251 (2014). http://doi:10.1016/j.ijpharm.2013.12.036.

[21] Illangakoon, U. E.; Yu, D. G.; Ahmad, B. S.; Chatterton, N. P.; Williams, G. R.: 5-Fluorouracil loaded Eudragit fibers prepared by electrospinning. International Journal of Pharmaceutics, **495**, 895–902 (2015). http://doi:10.1016/j.ijpharm.2015.09.044.

[22] Aguilar, L. E.; Unnithan, A. R.; Amarjargal, A.; Tiwari, A. P.; Hong, S. T.; Park, C. H.; Kim, C. S.: Electrospun polyurethane/Eudragit® L100-55 composite mats for the pH dependent release of paclitaxel on duodenal stent cover application. International Journal of Pharmaceutics, **478**, 1–8 (2015). http://doi:10.1016/j.ijpharm.2014.10.057.

[23] Giram, P. S.; Shitole, A.; Nande, S. S.; Sharma, N.; Garnaik, B.: Fast dissolving moxifloxacin hydrochloride antibiotic drug from electrospun Eudragit L-100 nonwoven nanofibrous Mats. Materials Science and Engineering C, **92**, 526–539 (2018). http://doi:10.1016/j.msec.2018.06.031.

[24] Fernández, S.; Guillén, M. de L.; López, R. G.; Enríquez-Medrano, F. J.; Cepeda, J.; Romero, J. C.; Saade, H.; Ilyna, A.: Biocompatible and Biodegradable Ultrafine

Nanoparticles of Poly(Methyl Methacrylate-co-Methacrylic Acid) Prepared via Semicontinuous Heterophase Polymerization: Kinetics and Product Characterization. International Journal of Polymer Science, **2016**, 1–8 (2016). http://doi:10.1155/2016/7674620.

[25] Greenley, R. Z.: Free radical copolymerization reactivity ratios. In *Polymer Handbook*; Brandrup, J., Immergut, E. H., Grulke, E. A., Eds.; John Wiley & Sons, Ltd: New York, (1999); pp. 181–308 ISBN 978-1-59124-883-5.

[26] Saade, H.; Diaz de León, R.; Enríquez-Medrano, F.J.; López, R.G.: Preparation of ultrafine poly(methyl methacrylate-co-methacrylic acid) biodegradable nanoparticles loaded with ibuprofen. Journal of Biomaterials Science, Polymer Edition, **27**, 1126-1138 (2016). http://dx.doi.org/10.1080/09205063.2016.1184120

[27] López-Muñoz, R.; Treviño, M.E.; Morales, G.; Valdez-Garza, J.A.; Díaz de León, R.; Saade, H.; Enríquez-Medrano, F.J.; López, R.G.: Ultrafine nanoparticles of poly(methyl methacrylate-co-methacrylic acid) loaded with aspirin. Journal of Nanomaterials, **2019**, 1-9 (2019). https://doi.org/10.1155/2019/3059098

[28] López-Muñoz, R.; Treviño, M.E.; Castellanos, F.; Morales, G.; Rodríguez-Fernández, O.; Saavedra, S.; Licea-Claverie, A.; Saade, H.; Enríquez-Medrano, F.J.; López, R.G.: Loading of doxorubicin on poly(methyl methacrylate-co-methacrylic acid) nanoparticles and release study. Journal of Biomaterials Science, Polymer Edition, **32**, 117-1124 (2021). https://doi.org/10.1080/09205063.2021.1900652

[29] Hejazi, I.; Sadeghi, G. M. M.; Jafari, S. H.; Khonakdar, H. A.; Seyfi, J.; Holzschuh, M.; Simon, F.: Transforming an intrinsically hydrophilic polymer to a robust self-cleaning superhydrophobic coating via carbon nanotube surface embedding. Materials and Design, **86**, 338–346 (2015). http://doi:10.1016/j.matdes.2015.07.092.

[30] Lee, M.; Lee, S.; Yim, C.; Jeon, S.: Surface wetting of superhydrophobic aluminum oxide nanostructures investigated using the fiber-optic spectrometer and quartz crystal microbalance. Sensors and Actuators, B: Chemical, **220**, 799–804 (2015). http://doi:10.1016/j.snb.2015.05.134.

[31] Park, S. C.; Yuan, Y.; Choi, K.; Choi, S. O.; Kim, J.: Doxorubicin release controlled by induced phase separation and use of a co-solvent. Materials, **11**, 1–14 (2018). http://doi:10.3390/ma11050681.

[32] Mansur, C. R. E.; Tavares, M. I. B.; Monteiro, E. E. C.: Thermal analysis and NMR studies of methyl methacrylate (MMA)-methacrylic acid copolymers synthesized by an unusual polymerization of MMA. Journal of Applied Polymer Science, **75**, 495–507

(2000). http://doi:10.1002/(SICI)1097-4628(20000124)75:4<495::AID-APP4>3.0.CO;2-R.

[33] Doustgani, A.: Doxorubicin release from optimized electrospun polylactic acid nanofibers. Journal of Industrial Textiles, **47**, 71–88 (2017). http://doi:10.1177/1528083716634033.

[34] Lanz-Landázuri, A.; Martínez De Ilarduya, A.; García-Alvarez, M.; Muñoz-Guerra, S.: Poly(β,L-malic acid)/Doxorubicin ionic complex: A pH-dependent delivery system. Reactive and Functional Polymers, **81**, 45–53 (2014). http://doi:10.1016/j.reactfunctpolym.2014.04.005.

[35] Wu, D. C.; Ofner, C. M.: Adsorption and degradation of doxorubicin from aqueous solution in polypropylene containers. AAPS PharmSciTech, **14**, 74–77 (2013). http://doi:10.1208/s12249-012-9885-1.

[36] Shoaib, M. H.; Tazeen, J.; Merchant, H. A.; Yousuf, R. I.: Evaluation of drug release kinetics from ibuprofen matrix tablets using HPMC. Pakistan Journal of Pharmaceutical Sciences, **19**, 119–124 (2006).